Glueballs at finite temperature in $SU(3)$ Yang-Mills theory

Xiang-Fei Meng,[1,2] Gang Li,[3,4] Yuan-Jiang Zhang,[3,4] Ying Chen,[3,4] Chuan Liu,[5] Yu-Bin Liu,[1]
Jian-Ping Ma,[6] and Jian-Bo Zhang[7]

(CLQCD Collaboration)

[1]*School of Physics, Nankai University, Tianjin 300071, People's Republic of China*
[2]*National Supercomputing Center, Tianjin 300457, People's Republic of China*
[3]*Institute of High Energy Physics, Chinese Academy of Sciences, Beijing 100049, People's Republic of China*
[4]*Theoretical Center for Science Facilities, Chinese Academy of Sciences, Beijing 100049, People's Republic of China*
[5]*School of Physics, Peking University, Beijing 100871, People's Republic of China*
[6]*Institute of Theoretical Physics, Chinese Academy of Sciences, Beijing 100080, People's Republic of China*
[7]*Department of Physics, Zhejiang University, Hangzhou, Zhejiang 310027, People's Republic of China*

Thermal properties of glueballs in $SU(3)$ Yang-Mills theory are investigated in a large temperature range from $0.3T_c$ to $1.9T_c$ on anisotropic lattices. The glueball operators are optimized for the projection of the ground states by the variational method with a smearing scheme. Their thermal correlators are calculated in all 20 symmetry channels. It is found in all channels that the pole masses M_G of glueballs remain almost constant when the temperature is approaching the critical temperature T_c from below, and start to reduce gradually with the temperature going above T_c. The correlators in the 0^{++}, 0^{-+}, and 2^{++} channels are also analyzed based on the Breit-Wigner *Ansatz* by assuming a thermal width Γ to the pole mass ω_0 of each thermal glueball ground state. While the values of ω_0 are insensitive to T in the whole temperature range, the thermal widths Γ exhibit distinct behaviors at temperatures below and above T_c. The widths are very small (approximately a few percent of ω_0 or even smaller) when $T < T_c$, but grow abruptly when $T > T_c$ and reach values of roughly $\Gamma \sim \omega_0/2$ at $T \approx 1.9T_c$.

I. INTRODUCTION

The past two or three decades witnessed intensive and extensive studies on the phase transition of quantum chromodynamics (QCD) [1], which is believed to be the fundamental theory of strong interaction. Based on the two characteristics of QCD, namely, the conjectured color confinement at low energies and the asymptotic freedom of gluons and quarks at high energies, QCD at finite temperature is usually described by two extreme pictures. One is with the weakly interacting meson gas in the low temperature regime and another is with perturbative quark-gluon plasma (QGP) in the high temperature regime. The two regimes are bridged by a deconfinement phase transition (or crossover). The study of the equation of state shows that the perturbative picture of QGP can only be achieved at very high temperatures $T \geq 2T_c$. In other words, the dynamical degrees of freedom up to the temperature of a few times of T_c are not just the quasifree gluons and quarks [2]. Some other theoretical studies also support this scenario and conjecture that in the intermediate temperature range above T_c there may exist different types of excitations corresponding to different distance scales [3,4] rendering the thermal states much more complicated. Apart from the quasifree quarks and gluons at the small distance scale, the large scale excitations can be

effective low-energy modes in the mesonic channels as a result of the strongly interacting partons [5]. The properties of the interaction among quarks and gluons at low and high temperatures can be studied with thermal correlators.

There have been many works on the correlators of charmonia at finite temperature. Phenomenological studies predicted the binding between quarks is reduced to dissolve J/ψ at temperatures close to T_c and proposed the suppression of charmonia as a signal of QGP [6,7]. For example, potential model studies show that excited states like ψ' and χ_c are dissociated at T_c, while the ground state charmonia J/Ψ and η_c survive up to $T = 1.1T_c$ [8–13]. However, it is unclear whether the potential model works well at finite temperatures [14]. In contrast, many recent numerical studies indicate that J/Ψ and η_c might still survive above $1.5T_c$ [15–19]. Of course, it is possible that the $\bar{c}c$ states observed in lattice QCD are just scattering states. A further lattice study on spatial boundary-condition dependence of the energy of low-lying $\bar{c}c$ systems concludes that they are spatially localized (quasi) bound states in the temperature region of $1.11 \sim 2.07T_c$ [20]. Obviously, the results of numerical lattice QCD studies are coincident to the picture of the QCD transition in the intermediate temperature regime.

Until now most of the lattice studies on hadronic correlators are in the quenched approximation. Because of the

lack of dynamical quarks in quenched QCD the binding of quark-antiquark systems must be totally attributed to the nonperturbative properties of gluons, which are the unique dynamical degree of freedom in the theory. Since glueballs are the bound states of gluons, a natural question is how glueballs respond to the varying temperatures. At low temperature $T \sim 0$, the existence of quenched glueballs has been verified by extensive lattice numerical studies, and their spectrum are also established quite well [21–28]. An investigation of the evolution of glueballs versus the increasing temperature is important to understand the QCD transition [29,30] and the hadronization of quark-gluon plasma [31]. From the point of view of QCD sum rules, glueball masses are closely related to the gluon condensate. Lattice studies [32] and model calculations [33] indicate that the gluon condensate keeps almost constant below T_c and reduces gradually with the increasing temperature above T_c. Based on this picture, it is expected intuitively that glueball masses should show a similar behavior also until they melt into gluons [34]. In fact, there has already been a lattice study on the scalar and tensor glueball properties at finite temperature [35]. In contrast to the expectation and the finite T behavior of charmonium spectrum, it is interestingly observed that the pole-mass reduction starts even below $T_c(m_G(T \sim T_c) \simeq 0.8m_G(T \sim 0))$. It is known that the spatial symmetry group on the lattice is the 24-element cubic point group O, whose irreducible representations are $R = A_1$, A_2, E, T_1, and T_2. Along with the parity P and charge conjugate transformation C, all the possible quantum numbers that glueballs can catch are R^{PC} with $PC = + +$, $- +$, $+ -$, and $+ +$, which add up to 20 symmetry channels. Motivated by the different temperature behaviors of $\bar{c}c$ systems with different quantum numbers, we would like to investigate the temperature dependence of glueballs in this paper.

Our numerical study in this work is carried out on anisotropic lattices with much finer lattice in the temporal direction than in spatial ones. In order to explore the temperature evolution of glueball spectrum, the temperature range studied here extends from $0.3T_c$ to $1.9T_c$, which is realized by varying the temporal extension of the lattice. Using anisotropic lattices, the lattice parameters are carefully determined so that there are enough time slices for a reliable data analysis even at the highest temperature. In the present study, we are only interested in the ground state in each symmetry channel R^{PC}. For the study optimized glueball operators that couple mostly to the ground states are desired. Practically, these optimized operators are built up by the combination of smearing schemes and the variational method [21–23]. In the data processing, the correlators of these optimized operators are analyzed through two approaches. First, the thermal masses M_G of glueballs are extracted in all the channels and all over the temperature range by fitting the correlators with a single-cosh function form, as is done in the standard hadron mass measure-

ments. Thus the T evolution of the thermal glueball spectrums is obtained. Secondly, with respect that the finite temperature effects may result in mass shifts and thermal widths of glueballs, we also analyze the correlators in A_1^{++}, A_1^{-+}, E^{++}, and T_2^{++} channels with the Breit-Wigner *Ansatz* which assumes these glueball thermal widths, say, change M_G into $\omega_0 - i\Gamma$ in the spectral function (see below). As a result, the temperature dependence of ω_0 and Γ can shed some light on the scenario of the QCD transition.

This paper is organized as follows. In Sec. II, a description of the determination of working parameters, such as the critical temperature T_c, temperature range, and lattice spacing a_s, as well as a brief introduction to the variational method is given. In Sec. III, after a discussion of its feasibility, the results of the single-cosh fit to the thermal correlators are described in detail. The procedure of the Breit-Wigner fit is also given in this section. Section IV gives the conclusion and some further discussions.

II. NUMERICAL DETAILS

For heavy particles such as charmonia and glueballs, the implementation of anisotropic lattices is found to be very efficient in the previous numerical lattice QCD studies both at low and finite temperatures. On the other hand, the Symanzik improvement and tadpole improvement schemes of the gauge action are verified to have better continuum extrapolation behaviors for many physical quantities. In other words, the finite lattice spacing artifacts are substantially reduced by these improvements. With these facts, we adopt the following improved gauge action which has been extensively used in the study of glueballs [21–23],

$$S_{\mathrm{IA}} = \beta\left[\frac{5}{3}\frac{\Omega_{\mathrm{sp}}}{\xi u_s^4} + \frac{4}{3}\frac{\xi\Omega_{\mathrm{tp}}}{u_t^2 u_s^2} - \frac{1}{12}\frac{\Omega_{\mathrm{sr}}}{\xi u_s^6} - \frac{1}{12}\frac{\xi\Omega_{\mathrm{str}}}{u_s^4 u_t^2}\right], \quad (1)$$

where β is related to the bare QCD coupling constant, $\xi = a_s/a_t$ is the aspect ratio for anisotropy (we take $\xi = 5$ in this work), u_s and u_t are the tadpole improvement parameters of spatial and temporal gauge links, respectively. $\Omega_C = \sum_C \frac{1}{3} \operatorname{Re} \operatorname{Tr}(1 - W_C)$, with W_C denoting the path-ordered product of link variables along a closed contour C on the lattice. Ω_{sp} includes the sum over all spatial plaquettes on the lattice, Ω_{tp} includes the temporal plaquettes, Ω_{sr} denotes the product of link variables about planar 2×1 spatial rectangular loops, and Ω_{str} refers to the short temporal rectangles (one temporal link, two spatial). Practically, u_t is set to 1, and u_s is defined by the expectation value of the spatial plaquette, $u_s = \langle\frac{1}{3}\operatorname{Tr}P_{ss'}\rangle^{1/4}$.

A. Determination of critical temperature

Since the temperature T on the lattice is defined by

$$T = \frac{1}{N_t a_t}, \quad (2)$$

where N_t is the temporal lattice size, T can be changed by varying either N_t or the coupling constant β, which is related directly to the lattice spacing. In order for the critical temperature to be determined with enough precision, for a given $N_t = 24$, we first determine the critical coupling β_c, because β can be changed continuously. The order parameter is chosen as the susceptibility χ_P of the Polyakov line, which is defined as

$$\chi_P = \langle \Theta^2 \rangle - \langle \Theta \rangle^2, \tag{3}$$

where Θ is the $Z(3)$ rotated Polyakov line,

$$\Theta = \begin{cases} \mathrm{Re}P \exp[-2\pi i/3] & \arg P \in [\pi/3, \pi) \\ \mathrm{Re}P & \arg P \in [-\pi/3, \pi/3) \\ \mathrm{Re}P \exp[2\pi i/3] & \arg P \in [-\pi, -\pi/3), \end{cases} \tag{4}$$

and P represents the trace of the spatially averaged Polyakov line on each gauge configuration.

After a β scanning on $L^4 = 24^4$ anisotropic lattices with $\xi = 5$, the critical point is trapped in a very narrow window $\beta_c \in [2.800, 2.820]$. In order to determine T_c more precisely, a more refined study is carried out in the β window mentioned above with much larger statistics through the spectral density method. Practically, the spectral density method [36,37] is applied to extrapolate the simulated χ_P's at $\beta = 2.805$, 2.810, and 2.815. In Table I are the numbers of heat-bath sweeps for each β. The extrapolation results are illustrated in Fig. 1 where the open triangles denote the simulated values of χ_P, while the filled squares are the extrapolated values. Finally, the peak position gives the critical coupling constant $\beta_c = 2.808$, which corresponds to the critical temperature $T_c \approx 0.724 r_0^{-1} = 296$ MeV with the lattice spacing $r_0/a_s = 3.476$ [38] and $r_0^{-1} = 410(20)$ MeV.

With T_c fairly determined, the working coupling constant β is set based on two requirements. First, the spatial volume of the lattice should be large enough in order for the glueballs to be free of any sizable finite volume effects. Secondly, we require that the temporal lattice has a good resolution even at the temperature $T \sim 2T_c$. Practically the working coupling constant is finally set to be $\beta = 3.2$. The lattice spacing at this β is set by calculating the static potential $V(r)$ on an anisotropic lattice $24^3 \times 128$. With the conventional parametrization of $V(r)$,

FIG. 1 (color online). The χ_P extrapolation based on the spectral density method. The open triangles denote the simulated values of χ_P, while the filled squares are the extrapolated values. The peak position gives the critical $\beta_c = 2.808$.

$$V(r) = V_0 + \sigma r + \frac{e_c}{r}, \tag{5}$$

the lattice spacing a_s is determined in the units of r_0 to be

$$\frac{a_s}{r_0} = \sqrt{\frac{\sigma a_s^2}{1.65 + e_c}} = 0.1825(7), \tag{6}$$

where r_0 is the hadronic scale parameter. If we take $r_0^{-1} = 410(20)$ MeV, we have $a_s = 0.0878(4)$ fm. The spatial volume at $L = 24$ is therefore estimated to be $(2.1$ fm$)^3$. On the other hand, using $T_c = 296$ MeV obtained at $\beta = 2.808$ as a rough estimate of T_c and ignoring the systematic error due to finite lattice spacings, T_c and $2T_c$ at $\beta = 3.2$ are expected to be achieved around $N_t \sim 40$ and $N_t \sim 20$, respectively. Obviously, the above two requirements are all satisfied.

Based on the discussions above, with a fixed $\beta = 3.2$, the calculations of the thermal correlators of glueballs are carried out on a series of lattice $24^3 \times N_t$ with $N_t = 20, 24, 28, 32, 36, 40, 44, 48, 60, 80,$ and 128, which cover the temperature range $0.3T_c < T < 2T_c$. As a cross-check, χ_P at different N_t are calculated first and the results are shown in Fig. 2 and Table II. It is clear that the expectation value of the Polyakov line drops to zero near $N_t = 40$ and the peak position of χ_P, which gives the critical temperature, is trapped between $N_t = 36$ and $N_t = 40$. In practice, we do not carry out a precise determination of T_c at $\beta = 3.2$, but take the temperature at $N_t = 38$, $T \approx (38a_t)^{-1} = (38a_s/\xi)^{-1} = 296$ MeV, as an approximation of $T_c(\beta = 3.2)$, to scale the temperatures involved in this work. It should be noted that, owing to the lattice artifact, the critical temperature T_c determined at different lattice spacings (or β) may differ from each other. The closeness of

TABLE I. The simulation parameters for the determination of the critical point. The configurations are selected every ten sweeps.

β	Total configurations	Thermalization	Bin size
2.80	20 000	5000	1000
2.805	30 000	10 000	1000
2.81	30 000	10 000	1000
2.815	20 000	5000	1000
2.82	8000	3000	500
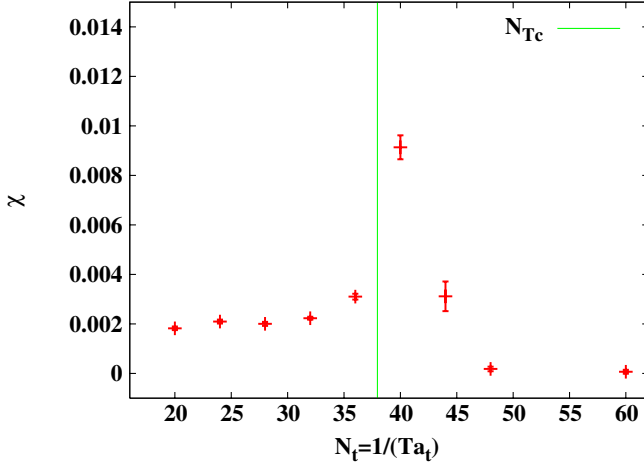
FIG. 2 (color online). χ_P is plotted versus N_t at $\beta = 3.2$. There is a peak of χ_P near $N_t = 40$.

$T_c(\beta = 2.808)$ and $T_c(\beta = 3.2)$ may signal that the lattice spacing dependence of T_c is mild in this work due to the application of the improved gauge action.

B. Variational method

It is known that many states contribute to a hadronic two-point function. Ideally one can extract the information of the lowest-lying states from the two-point function in the large time region if it lasts long enough in the time direction. This is the case for some light hadron states, such as π meson, K meson, etc. However, for heavy particles, especially for glueballs whose correlation functions are much more noisy than that of conventional hadrons made up of quarks, their two-point functions damp so fast with time that they are always undermined by noise rapidly before the ground states dominate. Practically, in the study of the glueball sector, in order to enhance the overlap of the glueball operators to the ground state, the commonly used techniques are the smearing schemes and the variational techniques. In this work, we adopt the sophisticated strat-

egy implemented by the studies of the zero-temperature glueball spectrum [21–23], which is outlined below. First, for each gauge configuration, we perform six smearing/ fuzzing schemes to the spatial links, which are various combinations of the single-link procedure (smearing) and the double-link procedure (fuzzing)

$$U_j^s(x) = P_{SU(3)}\left\{U_j(x) + \lambda_s \sum_{\pm(k \neq j)} U_k(x)U_j(x+\hat{k})U_k^\dagger(x+\hat{j})\right\},$$

$$U_j^f(x) = P_{SU(3)}\left\{U_j(x)U_j(x+\hat{j}) + \lambda_f \sum_{\pm(k \neq j)} U_k(x)U_j(x+\hat{k})\right.$$

$$\left. \times U_j(x+\hat{j}+\hat{k})U_k(x+2\hat{j})\right\}, \tag{7}$$

where $P_{SU(3)}$ denotes the projection into $SU(3)$ and is realized by the Jacobi method [39]. The six schemes are given explicitly as $s_{\lambda_s}^{10}$, $s_{\lambda_s}^{18}$, $s_{\lambda_s}^{26}$, $f_{\lambda_f} \otimes s_{\lambda_s}^{10}$, $f_{\lambda_f} \otimes s_{\lambda_s}^{18}$, $f_{\lambda_f} \otimes s_{\lambda_s}^{26}$, where s/f denotes the smearing/fuzzing procedure defined in Eq. (7), and λ_s/λ_f the tunable parameter which we take $\lambda_s = 0.1$ and $\lambda_f = 0.5$ in this work. Secondly, we choose the same prototype Wilson loops as that in Ref. [22] (as shown in Fig. 3), such that for each smearing/fuzzing scheme, all the different spatially oriented copies of these prototypes are calculated from the smeared gauge configurations. Thus for a given irreducible representation R of the spatial symmetry group O, say, $R = A_1$, A_2, E, T_1, or T_2, a realization of R can be a specific combination of differently oriented Wilson loops generated from the same prototype loop (one can refer to Ref. [23] for the concrete combinational coefficients). The glueball operators ϕ with the quantum number R^{PC} are thereby constructed along with the spatial reflection and the time inversion operations. In practice, we establish four realizations of each R^{PC} which are based on four different prototypes, respectively. Therefore, along with the six smearing/fuzzing schemes, an operator set of the

TABLE II.   Listed are the parameters used to check the critical behavior for $\beta = 3.2$. The configurations are selected every ten sweeps.

N_t	Total configurations	Thermalization	$\langle P \rangle$	χ_P
60	2000	500	-8.73×10^{-5}	6.65×10^{-5}
48	2000	500	6.01×10^{-5}	1.81×10^{-4}
44	8000	2000	2.25×10^{-3}	3.12×10^{-3}
40	8000	2000	1.72×10^{-2}	9.14×10^{-3}
36	8000	2000	5.21×10^{-2}	3.10×10^{-3}
32	3000	1000	8.51×10^{-2}	2.23×10^{-3}
28	2000	500	0.1253	2.00×10^{-3}
24	2000	500	0.1817	2.09×10^{-3}
20	2000	500	0.2571	1.82×10^{-3}
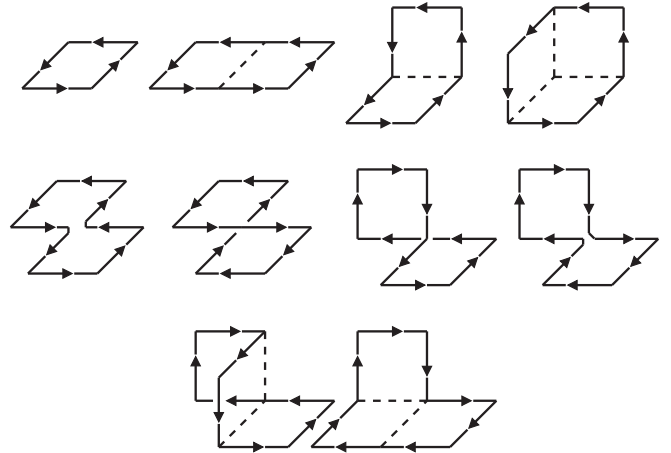
FIG. 3.   Prototype Wilson loops used in making the smeared glueball operators [22].

same specific quantum number R^{PC} is composed of 24 different operators, $\{\phi_\alpha, \alpha = 1, 2, \ldots, 24\}$. The last step is the implementation of the variational method (VM). The main goal of VM is to find an optimal combination of the set of operators, $\Phi = \sum v_\alpha \phi_\alpha$, which overlaps most to a specific state (in this work, we only focus on the ground states). The combinational coefficients $\mathbf{v} = \{v_\alpha, \alpha = 1, 2, \ldots, n\}$ can be obtained by minimizing the effective mass,

$$\tilde{m}(t_D) = -\frac{1}{t_D} \ln \frac{\sum_{\alpha\beta} v_\alpha v_\beta \tilde{C}_{\alpha\beta}(t_D)}{\sum_{\alpha\beta} v_\alpha v_\beta \tilde{C}_{\alpha\beta}(0)}, \tag{8}$$

at $t_D = 1$, where $\tilde{C}_{\alpha\beta}(t)$ is the correlation matrix of the operator set,

$$\tilde{C}_{\alpha\beta}(t) = \sum_\tau \langle 0|\phi_\alpha(t+\tau)\phi_\beta(\tau)|0\rangle. \tag{9}$$

This is equivalent to solving the generalized eigenvalue equation

$$\tilde{C}(t_D)\mathbf{v}^{(R)} = e^{-t_D \tilde{m}(t_D)} \tilde{C}(0)\mathbf{v}^{(R)}, \tag{10}$$

and the eigenvector $\mathbf{v}$ gives the desired combinational coefficients. Thus, the optimal operator that couples most to a specific state (the ground state in this work) can be built up as

$$\Phi = \sum_\alpha v_\alpha \phi_\alpha, \tag{11}$$

whose correlator $C(t)$ is expected to be dominated by the contribution of this state.

III. DATA ANALYSIS OF THE THERMAL CORRELATORS OF GLUEBALLS

All 20 R^{PC} channels, with $R = A_1, A_2, E, T_1, T_2$ and $PC = ++, +-, -+, --$, are considered in the calculation of the thermal correlators of glueballs on anisotropic lattices mentioned in Sec. II. At each temperature, after 10 000 pseudo-heat-bath sweeps of thermalization, the measurements are carried out every three compound sweeps, with each compound sweep composed of one pseudo-heat-bath and five microcanonical overrelaxation sweeps. In order to reduce the possible autocorrelations, the measured data are divided into bins of the size $n_{\mathrm{mb}} = 400$, and each bin is regarded as an independent measurement in the data analysis procedure. The numbers of bins N_{bin} and n_{mb} at various temperatures are listed in Table III.

Theoretically, under the periodic boundary condition in the temporal direction, the temporal correlators $C(t, T)$ at the temperature T can be written in the spectral representation as

TABLE III. Simulation parameters to calculate glueball spectrum. $\beta = 3.2$, $a_s = 0.0878$ fm, $L_s = 2.11$ fm.

N_t	T/T_c	n_{mb}	N_{bin}
128	0.30	400	24
80	0.47	400	30
60	0.63	400	44
48	0.79	400	40
44	0.86	400	44
40	0.95	400	40
36	1.05	400	40
32	1.19	400	56
28	1.36	400	40
24	1.58	400	40
20	1.90	400	40

$$C(t, T) \equiv \frac{1}{Z(T)} \mathrm{Tr}(e^{-H/T}\Phi(t)\Phi(0))$$

$$= \sum_{m,n} \frac{|\langle n|\Phi|m\rangle|^2}{2Z(T)} \exp\left(-\frac{E_m + E_n}{2T}\right)$$

$$\times \cosh\left[\left(t - \frac{1}{2T}\right)(E_n - E_m)\right]$$

$$= \int_{-\infty}^{\infty} d\omega \rho(\omega) K(\omega, T), \tag{12}$$

with a T-dependent kernel

$$K(\omega, T) = \frac{\cosh(\omega/(2T) - \omega t)}{\sinh(\omega/(2T))} \tag{13}$$

and the spectral function,

$$\rho(\omega) = \sum_{m,n} \frac{|\langle n|\Phi|m\rangle|^2}{2Z(T)} e^{-E_m/T}(\delta(\omega - (E_n - E_m))$$

$$- \delta(\omega - (E_m - E_n)), \tag{14}$$

where $Z(T)$ is the partition function at T, and E_n the energy of the thermal state $|n\rangle$ ($|0\rangle$ represents the vacuum state). In the zero-temperature limit ($T \to 0$), due to the factor $\exp(-E_m/T)$, the spectral function $\rho(\omega)$ degenerates to

$$\rho(\omega) = \sum_n \frac{|\langle 0|\Phi|n\rangle|^2}{2Z(0)}(\delta(\omega - E_n) - \delta(\omega + E_n)), \tag{15}$$

thus we have the function form of the correlation function,

$$C(t, T = 0) = \sum_n W_n e^{-E_n \tau} \tag{16}$$

with $W_n = |\langle 0|\Phi|n\rangle|^2/Z(0)$.

However, for any finite temperature (this is always the case for finite lattices), all the thermal states with the nonzero matrix elements $\langle m|\Phi|n\rangle$ may contribute to the spectral function $\rho(\omega)$. Intuitively in the confinement phase, the fundamental degrees of freedom are hadronlike modes; thus the thermal states should be multihadron

states. If they interact weakly with each other, we can treat them as free particles at the lowest order approximation and consider E_m as the sum of the energies of hadrons including in the thermal state $|m\rangle$. Since the contribution of a thermal state $|m\rangle$ to the spectral function is weighted by the factor $\exp(-E_m/T)$, apart from the vacuum state, the maximal value of this factor is $\exp(-M_{\min}/T)$ with $M_{\min}$ the mass of the lightest hadron mode in the system. As far as the quenched glueball system is concerned, the lightest glueball is the scalar, whose mass at the low temperature is roughly $M_{0^{++}} \sim 1.6$ GeV, which gives a very tiny weight factor $\exp(-M_{0^{++}}/T_c) \sim 0.003$ at T_c in comparison with unity factor of the vacuum state. That is to say, for the quenched glueballs, up to the critical temperature T_c, the contributions of higher spectral components beyond the vacuum to the spectral function are much smaller than the statistical errors (the relative statistical errors of the thermal glueball correlators are always a few percent) and can be neglected. As a result, the function form of $\rho(\omega)$ in

Eq. (15) can be a good approximation for the spectral function of glueballs at least up to T_c. Accordingly, considering the finite extension of the lattice in the temporal direction, the function form of the thermal correlators can be approximated as

$$C(t, T) = \sum_n W_n \frac{\cosh(M_n(1/(2T) - t))}{\sinh(M_n/(2T))}, \qquad (17)$$

which is surely the commonly used function form for the study of hadron masses at low temperatures on the lattice. As is always done, the glueball masses M_n derived by this function are called the pole masses in this work.

A. Results of the single-cosh fit

Even though the above discussions are based on the weak-interaction approximation for the hadronlike modes below T_c, we would like to apply Eq. (17) to analyzing the thermal correlators all over the temperature in concern.
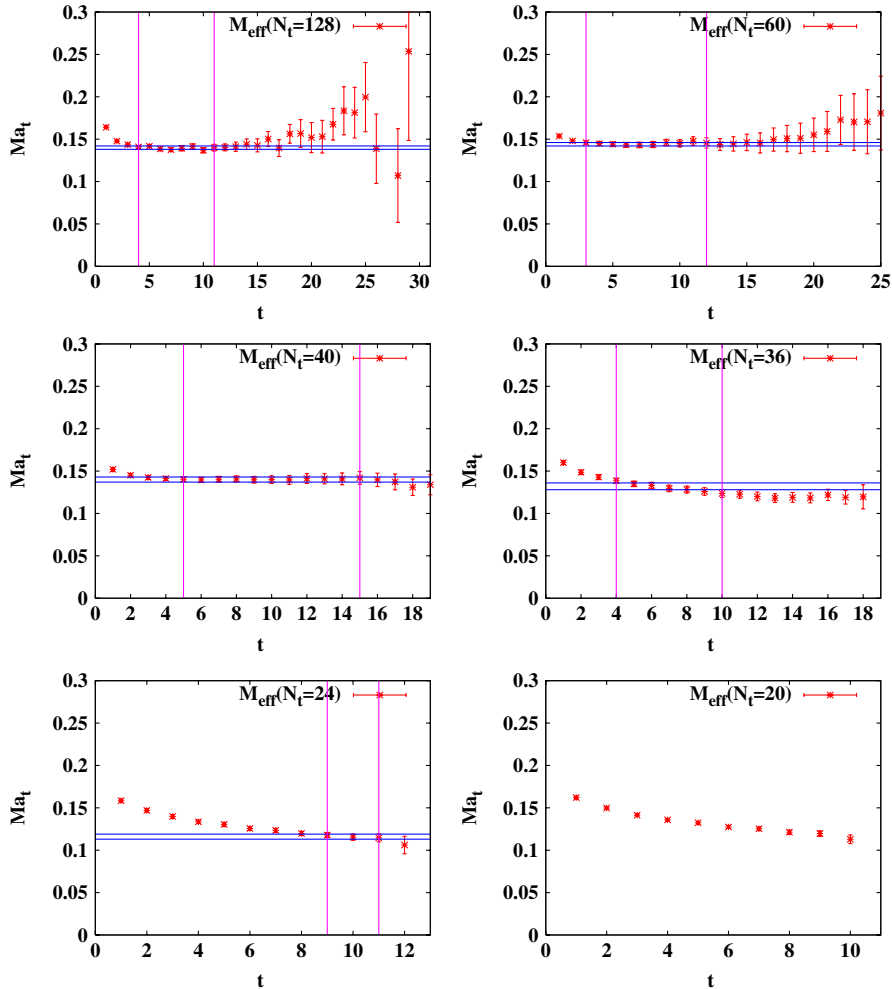
FIG. 4 (color online).   Effective masses at different temperatures in A_1^{++} channel. Data points are the effective masses with jackknife error bars. The vertical lines indicate the time window $[t_1, t_2]$ over which the single-cosh fittings are carried out, while the horizontal lines illustrate the best-fit result of pole masses (in each panel the double horizontal lines represent the error band estimated by jackknife analysis).

The interest of doing so is twofold. First, the thermal scattering of the glueball-like modes would result in a mass shift, say, the deviation of the pole mass from the glueball mass at zero temperature, which reflects the strength of the interaction at different temperature. Secondly, the breakdown of this function form would signal the dominance of new degrees of freedom instead of the hadronlike modes in the thermal states.

In practice, after the thermal correlators $C(t, T)$ of the optimal operators are obtained according to the steps described in Sec. II B, the pole masses of the ground state (or the lowest spectral component) can be extracted straightforwardly. First, for each R^{PC} channel and at each temperature T, the effective mass $M_{eff}(t)$ as a function of t is derived by solving the equation

$$\frac{C(t + 1, T)}{C(t, T)} = \frac{\cosh((t + 1 - N_t/2)a_t M_{eff}(t))}{\cosh((t - N_t/2)a_t M_{eff}(t))}. \quad (18)$$

Secondly, the effective masses are plotted versus t and the plateaus give the fit windows $[t_1, t_2]$. Finally, the pole masses of the ground states are obtained by fitting $C(t, T)$

through a single-cosh function form. As a convention in this work, we use M_G to represent the mass of a glueball state in the physical units and M to represent the dimensionless mass parameter in the data processing with the relation $M = M_G a_t$.

In Figs. 4–7 are shown the effective masses with jackknife errors at various temperatures in A_1^{++}, A_1^{-+}, E^{++}, and T_2^{++} channels, respectively. The vertical lines indicate the time window $[t_1, t_2]$ over which the single-cosh fittings are carried out, while the horizontal lines illustrate the best-fit result of pole masses (in each panel the double horizontal lines give the error band estimated by jackknife analysis). These figures exhibit some common features: At temperatures below T_c ($N_t = 128, 80, 40$), the effective mass plateaus show up almost right from the beginning of t, as it should be for the optimal glueball operators, while at $T > T_c$ ($N_t = 36, 24,$ and 20), the plateaus appear later and later in time, and even do not exist at $N_t = 20$ ($T = 1.90T_c$). This observation can be interpreted as follows. Since the effective masses are calculated based on Eq. (17), the very early appearance of the plateaus below
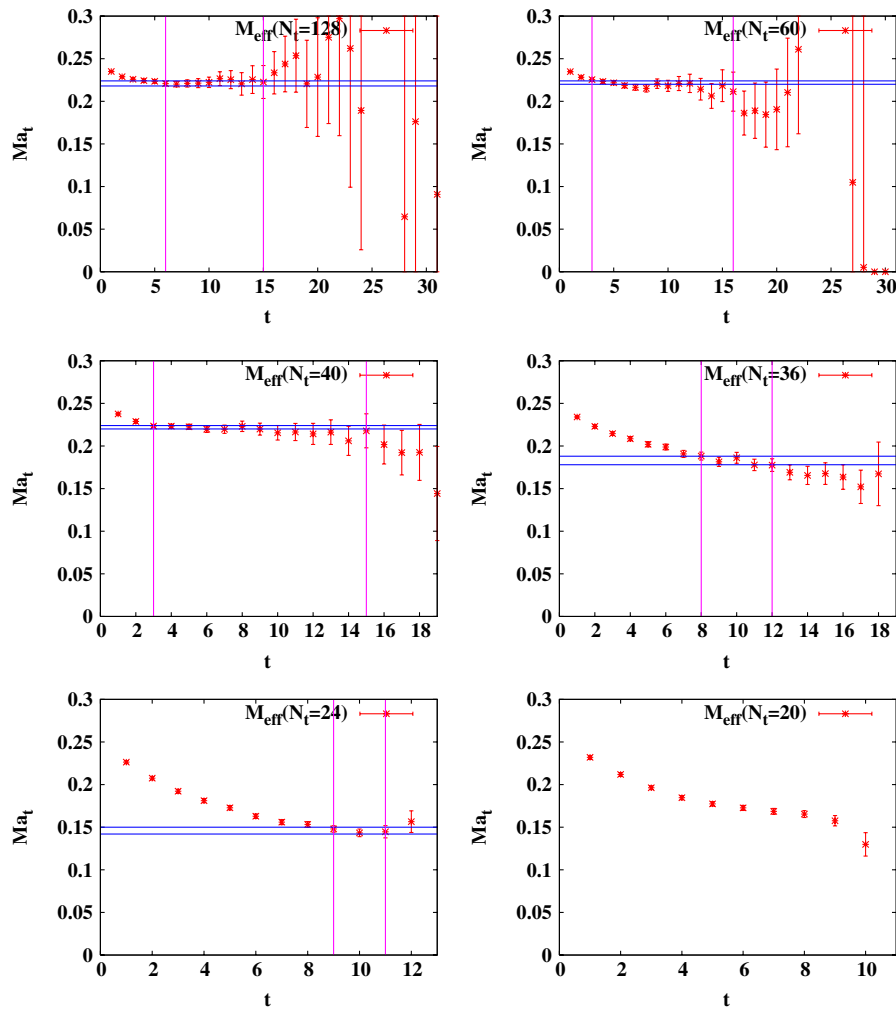
FIG. 5 (color online). Similar to Fig. 4, but in A_1^{-+} channel.
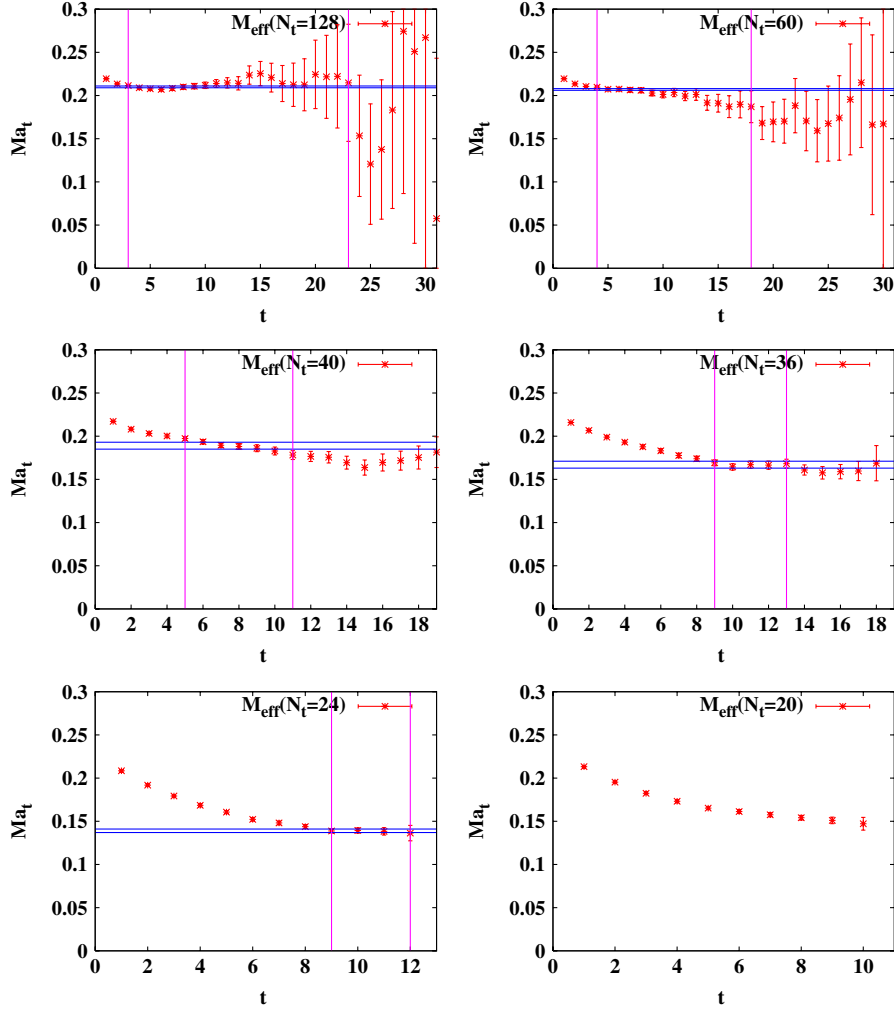
FIG. 6 (color online).   Similar to Fig. 4, but in E^{++} channel.

T_c implies that the thermal correlators $C(t, T)$ of the optimal operators are surely dominated by the ground state and can be well described by the function form of Eq. (17). In other words, the picture of weakly interacting glueball-like modes makes sense for the state of matter below T_c. While at $T > T_c$, the later appearance and the narrower size plateaus signal that the picture of the state of matter is distinct from that at $T < T_c$. However, because of the existence of effective mass plateaus up to $T \sim 1.58 T_c$ ($N_t = 24$), the possibility that glueball-like modes survive at this high temperature cannot be excluded.

The pole masses in all 20 R^{PC} channels are extracted in units a_t^{-1} at all temperatures and are shown in Table IV. Specifically, with the lattice spacing determined in Sec. II, the pole masses of A_1^{++}, A_1^{-+}, E^{++}, and T_2^{++} at $T \simeq 0$ in physical units are $M_{A_1^{++}} = 1.576(22)$ GeV, $M_{A_1^{-+}} = 2.488(34)$ GeV, $M_{E^{++}} \simeq M_{T_2^{++}} = 2.364(11)$ GeV, respectively, which are in agreement with that of previous studies [21–28]. From the table, one can see that the behaviors of the pole masses with respect to the temperature in all 20

channels are uniform: the pole masses keep almost constant with the temperature increasing from $0.30 T_c$ to right below T_c ($0.95 T_c$), and start to reduce gradually when $T > T_c$. When T increases up to $1.90 T_c$, the pole masses cannot be extracted reliably through the single-cosh fit for the lack of clear effective mass plateaus. Figure 8 illustrates these behaviors of pole masses in A_1^{++}, A_1^{-+}, E^{++}, and T_2^{++} channels.

These results imply that glueballs can be very stable below T_c and survive up to $1.6 T_c$. This coincides with the thermal properties of heavy quarkonia observed by model calculation and lattice numerical studies [3–5,15–19,40,41], but is different from the observation of a previous lattice study on glueballs where the observed pole-mass reduction starts even at $T \simeq 0.8 T_c$ [35].

B. Breit-Wigner analysis

In the single-cosh analysis, it is seen that, when the temperature increases up to T_c, the thermal correlators can be well described by Eq. (17) and the pole masses of
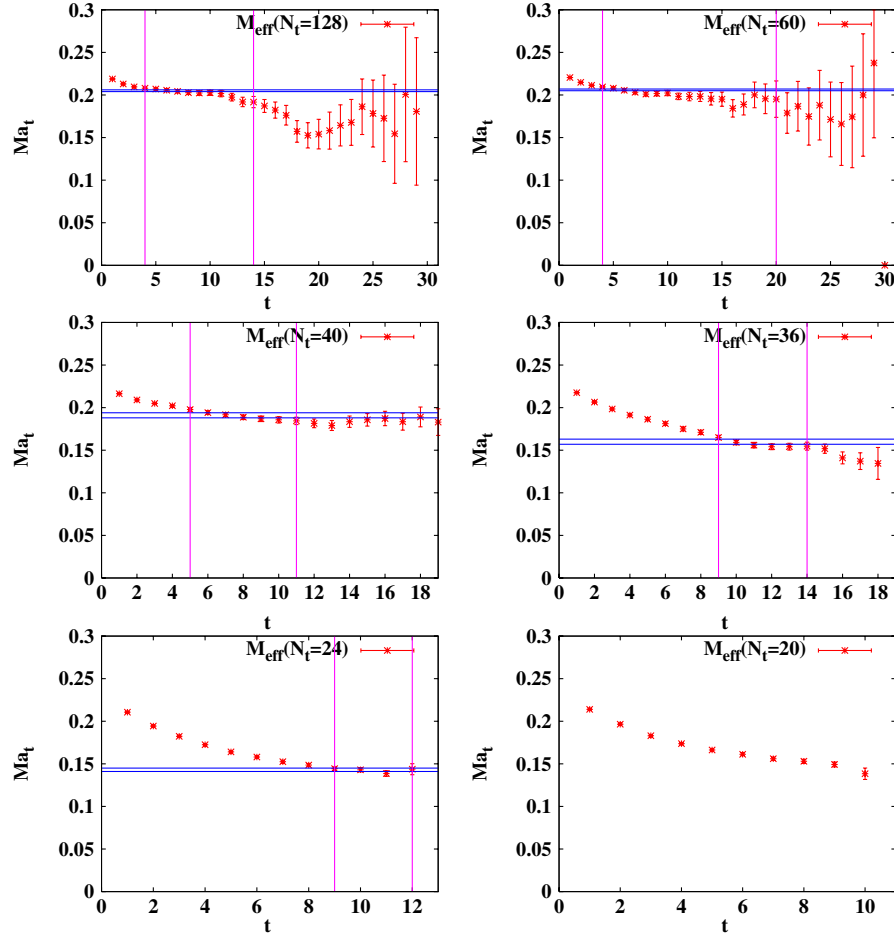
FIG. 7 (color online).   Similar to Fig. 4, but in T_2^{++} channel.

TABLE IV.   The pole masses (in units of a_t^{-1}) in all the 20 R^{PC} channels are extracted at all the temperatures.

R^{PC}	128	80	60	48	44	40	36	32	28	24
A_1^{++}	0.140(2)	0.144(3)	0.144(2)	0.143(3)	0.140(2)	0.140(3)	0.132(4)	0.126(2)	0.122(4)	0.116(3)
A_1^{+-}	0.441(3)	0.435(3)	0.434(5)	0.437(4)	0.432(4)	0.435(5)	0.399(6)	0.322(9)	0.267(16)	0.241(13)
A_1^{-+}	0.221(3)	0.225(2)	0.222(2)	0.225(2)	0.218(3)	0.222(2)	0.183(5)	0.174(3)	0.155(4)	0.146(4)
A_1^{--}	0.475(6)	0.453(8)	0.447(9)	0.464(7)	0.473(6)	0.468(6)	0.426(12)	0.417(10)	0.287(19)	0.253(18)
A_2^{++}	0.323(4)	0.327(4)	0.326(4)	0.330(2)	0.326(4)	0.332(3)	0.282(7)	0.249(8)	0.224(9)	0.208(9)
A_2^{+-}	0.302(5)	0.308(3)	0.308(5)	0.312(3)	0.312(5)	0.308(6)	0.268(6)	0.241(7)	0.220(8)	0.201(6)
A_2^{-+}	0.450(5)	0.449(7)	0.446(5)	0.440(6)	0.452(4)	0.448(5)	0.396(10)	0.340(11)	0.330(12)	0.250(14)
A_2^{--}	0.387(3)	0.388(3)	0.385(4)	0.390(5)	0.376(4)	0.375(4)	0.354(7)	0.293(7)	0.268(10)	0.214(9)
E^{++}	0.210(1)	0.205(1)	0.207(1)	0.209(2)	0.206(1)	0.189(4)	0.167(4)	0.153(3)	0.143(3)	0.139(2)
E^{+-}	0.401(2)	0.403(2)	0.401(2)	0.394(4)	0.400(2)	0.395(3)	0.375(4)	0.311(6)	0.261(7)	0.230(7)
E^{-+}	0.273(1)	0.266(1)	0.264(2)	0.273(2)	0.275(1)	0.262(2)	0.218(4)	0.196(4)	0.183(4)	0.181(4)
E^{--}	0.374(1)	0.368(2)	0.360(2)	0.361(3)	0.363(3)	0.352(4)	0.308(8)	0.262(6)	0.231(6)	0.213(6)
T_1^{++}	0.327(2)	0.326(4)	0.327(2)	0.334(2)	0.331(2)	0.312(5)	0.287(7)	0.266(3)	0.227(6)	0.215(4)
T_1^{+-}	0.278(1)	0.274(2)	0.265(3)	0.278(2)	0.281(1)	0.261(3)	0.207(6)	0.199(2)	0.181(4)	0.175(2)
T_1^{-+}	0.372(2)	0.377(4)	0.371(3)	0.380(2)	0.374(2)	0.370(3)	0.331(5)	0.289(7)	0.248(7)	0.230(5)
T_1^{--}	0.350(4)	0.349(2)	0.344(3)	0.351(2)	0.350(2)	0.343(3)	0.272(8)	0.252(5)	0.212(6)	0.201(5)
T_2^{++}	0.205(1)	0.209(1)	0.206(1)	0.205(1)	0.207(2)	0.191(3)	0.160(3)	0.152(2)	0.148(2)	0.143(2)
T_1^{+-}	0.322(2)	0.317(2)	0.310(4)	0.317(3)	0.320(2)	0.303(5)	0.276(5)	0.250(3)	0.201(4)	0.190(4)
T_1^{-+}	0.265(2)	0.260(3)	0.264(2)	0.273(3)	0.272(2)	0.264(2)	0.240(3)	0.213(3)	0.187(4)	0.183(4)
T_1^{--}	0.368(2)	0.358(3)	0.364(3)	0.358(4)	0.367(2)	0.353(5)	0.282(13)	0.254(6)	0.235(6)	0.220(4)
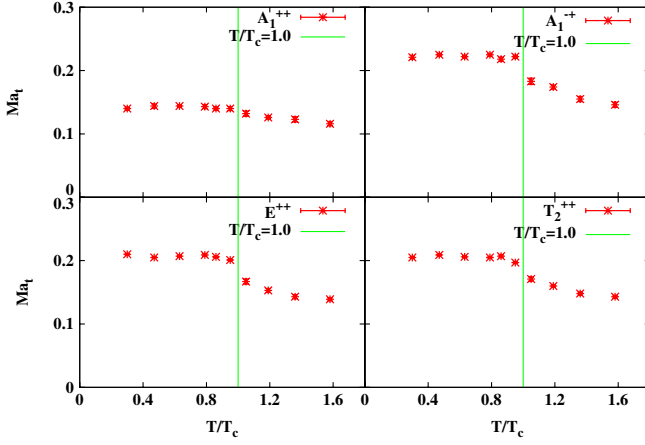
FIG. 8 (color online). The T dependence of pole masses A_1^{++}, A_1^{-+} E^{++}, and T_2^{++} glueballs.

glueballs are insensitive to T. This is in agreement with the picture that the states of matter below T_c are made up of weakly interacting glueball-like modes. When $T > T_c$, the thermal correlators deviate from Eq. (17) more and more. This observation implies that the degrees of freedom are very different from that when $T < T_c$. Theoretically, in the deconfined phase, gluons can be liberated from hadrons. However, the study of the equation of state shows that the state of the matter right above T_c is far from a perturbative gluon gas. In other words, the gluons in the intermediate temperature above T_c may interact strongly with each other and glueball-like resonances can possibly be formed. Thus different from bound states at low temperature, thermal glueballs can acquire thermal width due to the thermal scattering between strongly interacting gluons, and the magnitudes of the thermal widths can signal the strength of these types of interactions at different temperatures.

In order to take the thermal width into consideration, we also adopt the Breit-Wigner *Ansatz*, which is suggested by the pioneering work Ref. [35], to analyze the thermal correlators once more. First, we treat thermal glueballs as resonance objects which correspond to the poles (denoted by $\omega = \omega_0 - i\Gamma$) of the retarded and advanced Green functions in the complex ω plane (note that conventionally in particle physics, a resonance pole is always denoted as $M - i\Gamma/2$ where M is the mass of the resonance and Γ is its width). ω_0 is called the mass of the resonance glueball and Γ its thermal width in this work. Secondly, we assume that the spectral function $\rho(\omega)$ is dominated by these resonance glueballs. Thus the spectral function is parametrized as

$$\rho(\omega) = A(\delta_\Gamma(\omega - \omega_0) - \delta_\Gamma(\omega + \omega_0) + \cdots, \quad (19)$$

where δ_ϵ is the Lorentzian function

$$\delta_\epsilon(x) = \frac{1}{\pi} \text{Im}\left(\frac{1}{x - i\epsilon}\right) = \frac{1}{\pi} \frac{\epsilon}{x^2 + \epsilon^2}, \quad (20)$$

and "$\cdots$" represents the terms of excited states. With this spectral function, the thermal glueball correlator $G(t, T)$ can be expressed as

$$C(t, T) = \int_{-\infty}^{\infty} \frac{d\omega}{2\pi} \frac{\cosh(\omega(\frac{1}{2T} - t))}{2\sinh(\frac{\omega}{2T})} 2\pi A(\delta_\Gamma(\omega - \omega_0)$$
$$- \delta_\Gamma(\omega + \omega_0)) + \cdots. \quad (21)$$

The integral on the right-hand side of the above equation, denoted by $g_\Gamma(t)$, can be calculated explicitly as

$$g_\Gamma(t) = A\left[\text{Re}\left(\frac{\cosh((\omega_0 + i\Gamma)(\frac{1}{2T} - t))}{\sinh(\frac{(\omega_0 + i\Gamma)}{2T})} \right) \right.$$
$$+ 2\omega_0 T \sum_{n=1}^{\infty} \cos(2\pi nTt) \left\{ \frac{1}{(2\pi nT + \Gamma)^2 + \omega_0^2} \right.$$
$$\left. \left. - (n \to -n) \right\} \right], \quad (22)$$

which can be used as the fit function to extract ω_0 and Γ from the thermal correlators obtained from the numerical calculation. Practically, the infinite series in the above equation is truncated by setting the upper limit of the summation to be 50, which is tested to be enough for all the cases considered in this work.

In the present study, we carry out the Breit-Wigner analysis in A_1^{++}, A_1^{-+}, E^{++}, and T_2^{++} channels, whose continuum correspondences are 0^{++}, 0^{-+}, and 2^{++}. Although the variational method is exploited to enhance the contribution of the ground state to the thermal correlators, the contributions from higher spectral components cannot be eliminated completely. Therefore, the fit range must be chosen properly where the contribution of the ground state dominates. We take the strategy advocated in Ref. [35] as follows. For a given correlator $C(t, T)$, the effective peak position $\omega_0^{(\text{eff})}(t)$ and the effective width $\Gamma^{(\text{eff})}(t)$ are obtained by solving the equations

$$\frac{g_\Gamma(t)}{g_\Gamma(t + 1)} = \frac{C(t, T)}{C(t + 1, T)}, \qquad \frac{g_\Gamma(t + 1)}{g_\Gamma(t + 2)} = \frac{C(t + 1, T)}{C(t + 2, T)}. \quad (23)$$

The statistical errors of $\omega_0^{(\text{eff})}(t)$ and $\Gamma^{(\text{eff})}(t)$ can be estimated through the jackknife analysis. Thus the fit range, denoted by $[t_1, t_2]$, is chosen to be the time range where $\omega_0^{(\text{eff})}(t)$ and $\Gamma^{(\text{eff})}(t)$ show up plateaus simultaneously. For example, the procedure in T_2^{++} channel is illustrated in Fig. 9 for $N_t = 128, 36, 20$ (corresponding to the temperature $T/T_c = 0.30, 1.05, 1.90$), where the fit ranges $[t_1, t_2]$ are determined to include the time slices between the two vertical lines in each figure.

After the fit ranges for all the thermal correlators are chosen, the jackknife analysis can be carried out straightforwardly and the detailed procedures are omitted here. Tables V, VI, VII, and VIII show the fit windows $[t_1, t_2]$, the chi-square per degree of freedom $\chi^2/\text{d.o.f}$, and the best-fit

(a) (b) (c)
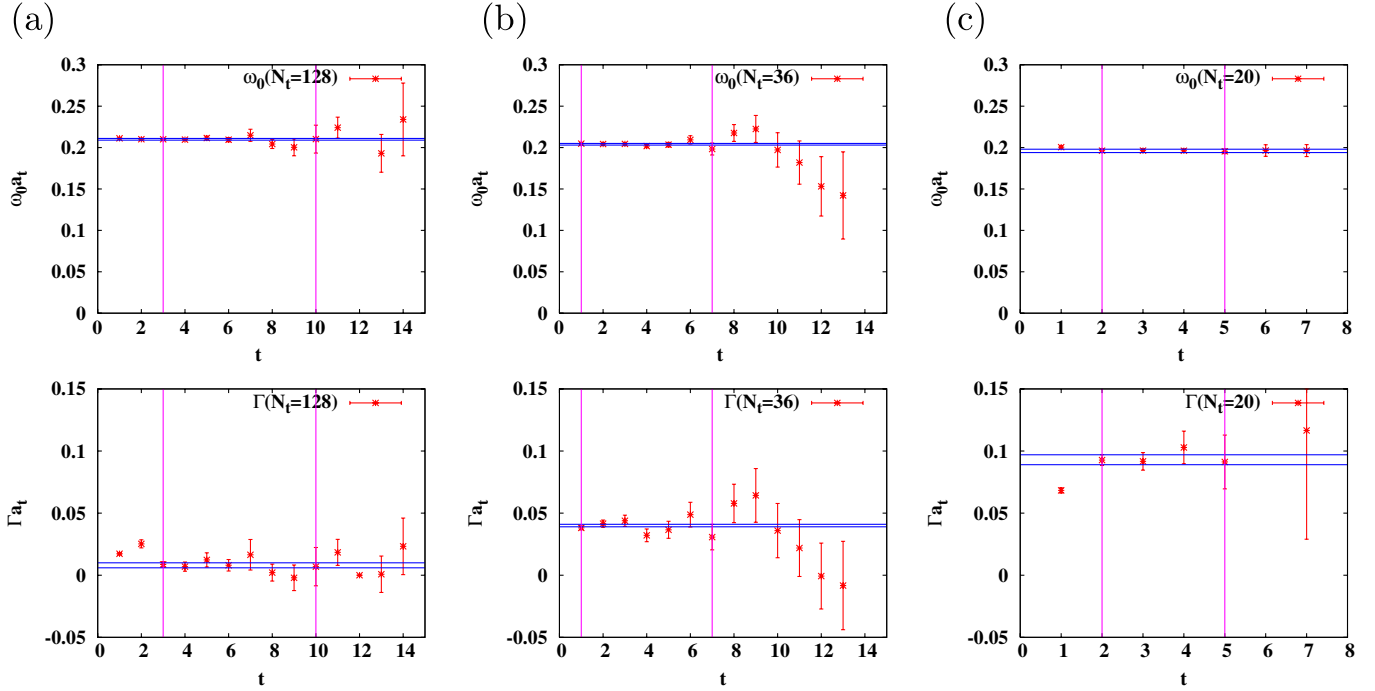
FIG. 9 (color online).   Determinations of the fit range $[t_1, t_2]$ in T_2^{++} channel at $N_t = 128$, 36, and 20. In each row, $\omega_0^{(\text{eff})}(t)$ and $\Gamma^{(\text{eff})}(t)$ obtained by solving Eq. (23) are plotted by data points with jackknife error bars. $[t_1, t_2]$ are chosen to include the time slices between the two vertical lines, where $\omega_0^{(\text{eff})}(t)$ and $\Gamma^{(\text{eff})}(t)$ show up plateaus simultaneously. The best-fit results of ω_0 and Γ through the function $g_\Gamma(t)$ are illustrated by the horizontal lines. (a) $N_t = 128(T/T_c = 0.32)$, (b) $N_t = 36(T/T_c = 1.09)$), and (c) $N_t = 20(T/T_c = 1.97)$.

results of ω_0 and Γ at various temperatures in A_1^{++}, A_1^{-+}, E^{++}, and T_2^{++} channels. In almost all the cases, the fit ranges start from $t_1 = 1$, 2, or 3, and last for quite a few time slices. This reflects that, as is expected, the optimal glueball operators couple almost exclusively to the lowest spectral components after the implementation of the variational method. All the $\chi^2/\text{d.o.f}$'s are $\sim O(1)$ or even smaller, which reflects the reliability of the fits.

The main features of the best fit ω_0 and Γ based on the Breit-Wigner *Ansatz* are described as follows:
(i) The peak positions ω_0 of the spectral functions $\rho(\omega)$ are insensitive to the temperature in all the considered channels. In particular, the ω_0 in A_1^{++} channel keeps almost constant all over the temperature range from $0.30T_c$ to $1.90T_c$. In the other three channels, the ω_0's do not change within errors below T_c, but reduce mildly with the increasing temperature above

TABLE V.   The best fit ω_0 and Γ of A_1^{++} channel at different T through the Breit-Wigner fit. Also listed are the fit window $[t_1, t_2]$ and the chi-square per degree of freedom, $\chi^2/\text{d.o.f.}$

N_t	T/T_c	ω_0	Γ	$[t_1, t_2]$	$\chi^2/\text{d.o.f}$
128	0.30	0.142(2)	0.008(10)	(3, 6)	1.266
80	0.47	0.146(2)	0.013(9)	(2, 4)	0.921
60	0.63	0.144(2)	0.008(3)	(2, 7)	0.135
48	0.79	0.143(2)	0.014(6)	(2, 4)	0.639
44	0.86	0.142(2)	0.004(3)	(1, 7)	0.758
40	0.95	0.143(2)	0.003(4)	(4, 7)	0.850
36	1.05	0.146(2)	0.028(4)	(3, 6)	0.960
32	1.19	0.141(2)	0.053(2)	(1, 4)	0.393
28	1.36	0.142(2)	0.056(4)	(2, 5)	1.253
24	1.58	0.143(1)	0.059(3)	(1, 4)	0.302
20	1.90	0.146(2)	0.077(5)	(2, 4)	0.918

TABLE VI.   The best fit ω_0 and Γ of A_1^{-+} channel at different T through the Breit-Wigner fit. Also listed are the fit window $[t_1, t_2]$ and the chi-square per degree of freedom, $\chi^2/\text{d.o.f.}$

N_t	T/T_c	ω_0	Γ	$[t_1, t_2]$	$\chi^2/\text{d.o.f}$
128	0.30	0.226(2)	0.006(5)	(3, 9)	0.509
80	0.47	0.228(2)	0.008(4)	(2, 6)	0.640
60	0.63	0.227(1)	0.013(5)	(2, 7)	0.216
48	0.79	0.228(2)	0.012(5)	(2, 6)	0.177
44	0.86	0.229(2)	0.013(4)	(2, 8)	0.184
40	0.95	0.224(2)	0.004(6)	(3, 6)	0.549
36	1.05	0.221(2)	0.037(3)	(1, 8)	0.935
32	1.19	0.219(2)	0.047(3)	(1, 6)	0.250
28	1.36	0.211(3)	0.068(6)	(2, 5)	0.091
24	1.58	0.208(3)	0.089(7)	(2, 4)	0.003
20	1.90	0.211(3)	0.099(9)	(2, 6)	0.083

TABLE VII.   The best-fit ω_0 and Γ of E^{++} channel at different T through the Breit-Wigner fit. Also listed are the fit window $[t_1, t_2]$ and the chi-square per degree of freedom, $\chi^2/\text{d.o.f.}$

N_t	T/T_c	ω_0	Γ	$[t_1, t_2]$	$\chi^2/\text{d.o.f.}$
128	0.30	0.212(1)	0.012(4)	(2, 5)	0.274
80	0.47	0.211(1)	0.006(3)	(2, 8)	0.616
60	0.63	0.212(1)	0.010(3)	(2, 9)	0.844
48	0.79	0.213(1)	0.011(3)	(2, 5)	0.206
44	0.86	0.211(1)	0.011(3)	(2, 8)	1.268
40	0.95	0.207(1)	0.022(3)	(2, 6)	0.250
36	1.05	0.205(2)	0.034(2)	(1, 8)	0.183
32	1.19	0.200(1)	0.049(2)	(1, 6)	0.478
28	1.36	0.191(2)	0.067(4)	(2, 6)	0.297
24	1.58	0.189(2)	0.083(5)	(2, 4)	0.253
20	1.90	0.196(2)	0.091(5)	(2, 4)	0.046

TABLE VIII.   The best fit ω_0 and Γ of T_2^{++} channel at different T through the Breit-Wigner fit. Also listed are the fit window $[t_1, t_2]$ and $\chi^2/\text{d.o.f.}$

N_t	T/T_c	ω_0	Γ	$[t_1, t_2]$	$\chi^2/\text{d.o.f}$
128	0.30	0.210(1)	0.008(2)	(3,10)	0.442
80	0.47	0.213(1)	0.009(3)	(3, 9)	0.696
60	0.63	0.213(1)	0.012(3)	(3, 7)	0.326
48	0.79	0.210(1)	0.007(4)	(3, 6)	0.288
44	0.86	0.214(1)	0.012(2)	(2, 6)	0.437
40	0.95	0.208(1)	0.023(1)	(1, 7)	0.743
36	1.05	0.204(1)	0.039(2)	(1, 7)	0.606
32	1.19	0.199(1)	0.047(1)	(1, 6)	0.527
28	1.36	0.196(2)	0.064(3)	(2, 5)	0.022
24	1.58	0.194(1)	0.077(4)	(2, 7)	0.119
20	1.90	0.196(2)	0.093(4)	(2, 5)	0.027

T_c. The reduction of ω_0 at the highest temperature $T = 1.90T_c$ is less than 5% in these three channels.

(ii) In all the four channels, the thermal widths Γ are small and do not vary much below T_c, but grow rapidly with the increasing temperature when $T > T_c$. Below T_c, the thermal widths are of order $\Gamma \sim$ 5% or even smaller (especially for the A_1^{++} Γ is consistent with zero). The thermal widths increase abruptly when the temperature passes T_c and reach values $\sim \omega_0/2$ at $T = 1.90T_c$.

These features can be seen easily in Figs. 10 and 11, where the behaviors of ω_0 and Γ with respect to the temperature T are plotted for all four channels. The line shapes of the spectral functions with the best-fit parameters at different T are shown in Fig. 12 for A_1^{-+}, E^{++}, and T_2^{++} channels (we do not plot the spectral function of A_1^{++} channel due to the small thermal widths).

IV. SUMMARY AND DISCUSSIONS

On $24^3 \times N_t$ anisotropic lattices with the anisotropy $\xi = 5$ at the gauge coupling $\beta = 3.2$, the thermal glueball correlators are calculated in a large temperature range from $0.30T_c$ to $1.90T_c$, which are realized by varying N_t to represent different temperatures. Based on the lattice spacing $a_s = 0.0878(4)$ fm determined by $r_0^{-1} = (410(20)$ MeV), the spatial extensions of the lattices are estimated to be $(2.1$ fm$)^3$, which is large enough to be free of the finite volume effects. On the other hand, because of the large anisotropy, there are enough data points in the temporal direction for the thermal correlators to be analyzed comfortably even at the highest temperature $T \sim 2T_c$ concerned in this work. With the implementation of the
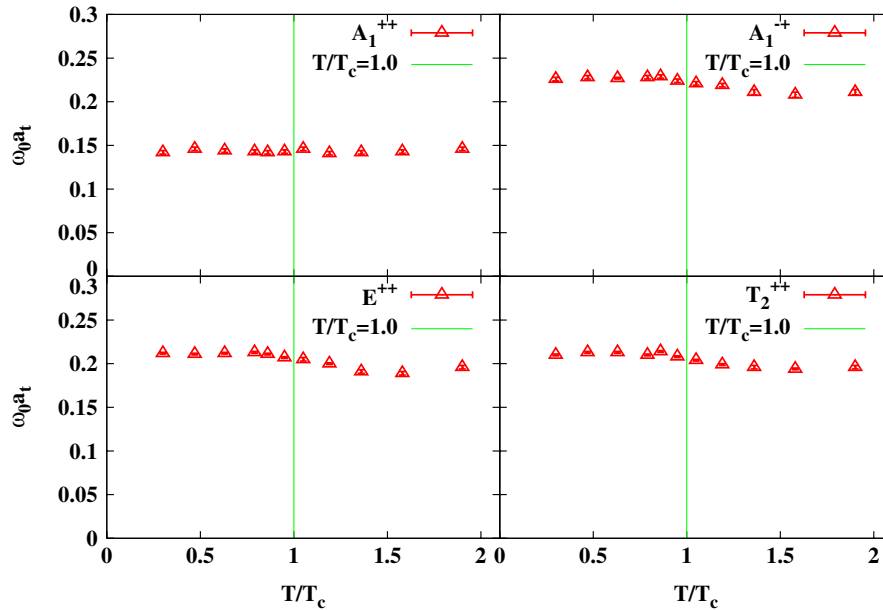
FIG. 10 (color online). ω_0's are plotted versus T/T_c for A_1^{++}, A_1^{-+} E^{++}, and T_2^{++} channels. The vertical lines indicate the critical temperature.
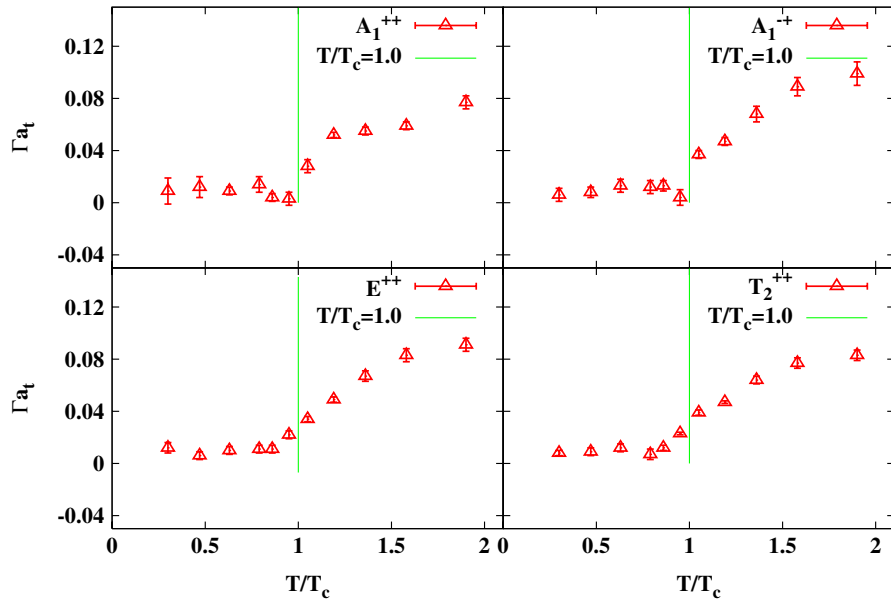
FIG. 11 (color online). Γ's are plotted versus T/T_c for A_1^{++}, A_1^{-+} E^{++}, and T_2^{++} channels. The vertical lines indicate the critical temperature.

smearing scheme and the variational method, we can construct the optimal glueball operators in all the symmetry channels, which couple mostly to the lowest-lying states (or more precisely, the lowest-lying spectral components). As a result, the thermal correlators of these operators can be considered to be contributed dominantly from these lowest-lying states. The thermal correlators are analyzed based on two *Ansätze*, say, the single-cosh function form and the Breit-Wigner *Ansatz*. In Tables IX and X, the "pole masses" M_G obtained by single-cosh analysis and (ω_0, Γ) obtained based on the Breit-Wigner *Ansatz* are combined together for comparison (all the data are converted into physical units).

The most striking observation from the single-cosh analysis is that, in all 20 R^{PC} channels, the best-fit pole masses M_G are almost constant within errors from the low temperature up to right below the critical temperature T_c.

This is what it should be from the point of view of the deconfinement phase transition of QCD: Since below T_c the system is in the confinement phase, the fundamental degrees of freedom must be hadrons. Above T_c, the reduction of the pole masses does signal the QCD transition, after which the state of the matter is very different from that below T_c. However, the existence of effective mass plateaus, from which the pole masses are extracted, also implies that color singlet objects, the glueball-like modes, can also survive at the intermediate temperature above T_c. The results of the Breit-Wigner fit are consistent with this picture. In the Breit-Wigner *Ansatz*, thermal widths Γ are introduced to glueball states to account for the effects of finite temperature, such as the thermal scattering and the thermal fluctuations. As shown in Tables IX and X, below T_c (or in the confinement phase), the best-fit ω_0's are very close to the pole masses, and the thermal widths Γ are very
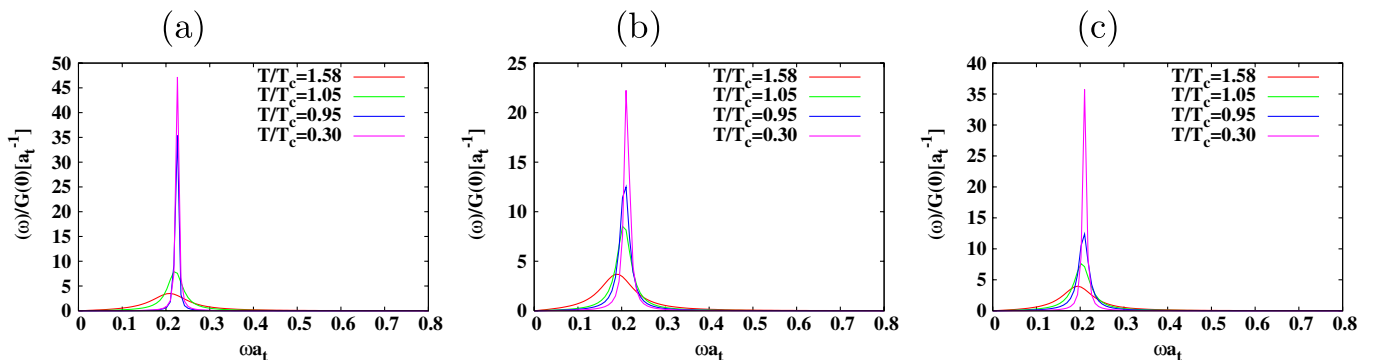
FIG. 12 (color online).   Plotted are the spectral function $\rho(\omega)$ at $T/T_c = 0.30$, 0.95, 1.05, and 1.58 with the best-fit parameters. Panels (a)–(c) are for A_1^{-+}, E^{++}, and T_2^{++} channels, respectively.

TABLE IX. The pole masses M_G obtained by single-cosh analysis and (ω_0, Γ) obtained based on the Breit-Wigner *Ansatz* are combined together for comparison. Listed in the table are the results in A_1^{++} and A_1^{-+} channels (all the data are converted into physical units).

| A_1^{++} | | | | | A_1^{-+} | | |
N_t	T/T_c	m_G [GeV]	ω_0 [GeV]	Γ [GeV]	m_G [GeV]	ω_0 [GeV]	Γ [GeV]
128	0.30	1.576(22)	1.602(14)	0.091(113)	2.488(31)	2.549(17)	0.069(52)
80	0.47	1.621(29)	1.644(22)	0.145(100)	2.533(24)	2.560(17)	0.086(44)
60	0.63	1.627(18)	1.621(16)	0.098(38)	2.499(27)	2.559(16)	0.147(54)
48	0.79	1.616(21)	1.612(26)	0.156(67)	2.533(23)	2.564(20)	0.135(55)
44	0.86	1.577(25)	1.598(17)	0.045(34)	2.454(34)	2.577(18)	0.144(48)
40	0.95	1.576(39)	1.621(20)	0.034(46)	2.499(25)	2.525(26)	0.042(71)
36	1.05	1.486(43)	1.638(28)	0.315(48)	2.060(48)	2.490(23)	0.413(32)
32	1.19	1.418(21)	1.588(25)	0.586(28)	1.959(37)	2.464(20)	0.529(28)
28	1.36	1.373(48)	1.599(26)	0.619(43)	1.745(43)	2.375(28)	0.768(71)
24	1.58	1.306(41)	1.613(28)	0.664(37)	1.644(45)	2.308(32)	0.999(83)
20	1.90	$\cdots$	1.642(32)	0.873(59)	$\cdots$	2.380(35)	1.114(99)

tiny and are always of a few percent of ω_0. This means the glueball states are surely stable in the confinement phase and the thermal interactions among them are weak. With the temperature increasing above T_c, while the temperature dependence of ω_0's is very mild, the thermal widths Γ grow rapidly and reach values of roughly half of ω's at $T \sim 1.9 T_c$. This clearly reflects that glueballs act as resonances are unstable more and more, and the reduction of pole masses above T_c can be taken as the effect of these growing thermal widths.

To summarize, in pure gauge theory, the state of matter is dominated by weakly interacting hadronlike states below T_c; when $T > T_c$, glueball states survive as resonancelike modes up to a temperature $T \sim 1.9 T_c$ with their thermal widths growing with increasing T, which implies that in this intermediate temperature range, glueballs are unstable and may decay into gluons, and reversely gluons also interact strongly enough to form glueball-like resonances.

The two procedures may reach the thermal equilibrium at a given temperature, such that the gluon degree of freedom becomes more and more important with T increasing. At very high temperature, the glueball-like resonances may disappear finally and the state of matter can thereby be described by a perturbative gluon plasma. This picture is coincident with the observations both in the study of equation of state of QCD and the thermal properties of heavy quarkonia. On the other hand, the surprising results of RHIC experiments may also support this picture to some extent. First, the data of RHIC experiments are well described by the hydrodynamical model [42]. Secondly, the investigation of elliptic flow data using a Boltzmann-type equation for gluon scattering is not consistent with the perturbative QCD apparently [43]. So the quark-gluon plasma at the RHIC temperature is most likely a strongly interacting system.

TABLE X. The pole masses M_G obtained by single-cosh analysis and (ω_0, Γ) obtained based on the Breit-Wigner *Ansatz* are combined together for comparison. Listed in the table are the results in E^{++} and T_2^{++} channels (all the data are converted into physical units).

| E^{++} | | | | | T_2^{++} | | |
N_t	T/T_c	m_G [GeV]	ω_0 [GeV]	Γ [GeV]	m_G [GeV]	ω_0 [GeV]	Γ [GeV]
128	0.30	2.364(11)	2.385(12)	0.140(42)	2.308(14)	2.363(10)	0.091(25)
80	0.47	2.308(13)	2.368(12)	0.069(29)	2.353(15)	2.387(10)	0.105(32)
60	0.63	2.330(11)	2.383(12)	0.116(32)	2.319(13)	2.396(10)	0.140(32)
48	0.79	2.353(19)	2.393(15)	0.129(34)	2.308(15)	2.362(14)	0.083(43)
44	0.86	2.319(15)	2.379(12)	0.119(32)	2.330(21)	2.405(10)	0.136(26)
40	0.95	2.263(14)	2.327(15)	0.247(38)	2.218(16)	2.344(11)	0.259(16)
36	1.05	1.880(41)	2.305(17)	0.382(23)	1.925(33)	2.298(14)	0.437(17)
32	1.19	1.722(35)	2.247(16)	0.549(20)	1.801(25)	2.244(11)	0.532(15)
28	1.36	1.610(31)	2.155(19)	0.754(43)	1.666(23)	2.205(17)	0.717(36)
24	1.58	1.565(23)	2.132(21)	0.937(55)	1.610(27)	2.184(16)	0.870(41)
20	1.90	$\cdots$	2.201(23)	1.023(60)	$\cdots$	2.209(20)	0.935(48)

[1] P. Petreczky, arXiv:hep-lat/0506012, and references therein; J. Schaffner-Bielich, Proc. Sci., CPOD07 (2007) 062 [arXiv:0709.1043], and references therein.

[2] F. Karsch, E. Laermann, and A. Peikert, Phys. Lett. B **478**, 447 (2000).

[3] S. Gottlieb, W. Liu, D. Toussaint, R. L. Renken, and R. L. Sugar, Phys. Rev. Lett. **59**, 2247 (1987); S. Gottlieb, W. Liu, R. L. Renken, R. L. Sugar, and D. Toussaint, Phys. Rev. D **38**, 2888 (1988); S. Gottlieb, U. M. Heller, A. D. Kennedy, S. Kim, J. B. Kogut, C. Liu, R. L. Renken, D. K. Sinclair, R. L. Sugar, D. Toussaint, and K. C. Wang, Phys. Rev. D **55**, 6852 (1997).

[4] C. DeTar, Phys. Rev. D **32**, 276 (1985); **37**, 2328 (1988).

[5] G. Boyd, S. Gupta, F. Karsch, and E. Laermann, Z. Phys. C **64**, 331 (1994).

[6] T. Matsui and H. Satz, Phys. Lett. B **178**, 416 (1986).

[7] T. Hashimoto, O. Miyamura, K. Hirose, and T. Kanki, Phys. Rev. Lett. **57**, 2123 (1986).

[8] F. Karsch, M. T. Mehr, and H. Satz, Z. Phys. C **37**, 617 (1988).

[9] S. Digal, P. Petreczky, and H. Satz, Phys. Lett. B **514**, 57 (2001).

[10] S. Digal, P. Petreczky, and H. Satz, Phys. Rev. D **64**, 094015 (2001).

[11] E. V. Shuryak and I. Zahed, Phys. Rev. D **70**, 054507 (2004).

[12] C.-Y. Wong, Phys. Rev. C **72**, 034906 (2005).

[13] Á. Mócsy and P. Petreczky, Eur. Phys. J. C **43**, 77 (2005); Phys. Rev. D **73**, 074007 (2006)

[14] P. Petreczky, Eur. Phys. J. C **43**, 51 (2005).

[15] M. Asakawa and T. Hatsuda, Phys. Rev. Lett. **92**, 012001 (2004).

[16] S. Datta, F. Karsch, P. Petreczky, and I. Wetzorke, Phys. Rev. D **69**, 094507 (2004); J. Phys. G **30**, S1347 (2004).

[17] H. Iida, T. Doi, N. Ishii, H. Suganuma, and K. Tsumura, Phys. Rev. D **74**, 074502 (2006).

[18] A. Jakovac, P. Petreczky, K. Petrov, and A. Velytsky, arXiv:hep-lat/0603005.

[19] B. Berg and A. Billoire, Nucl. Phys. **A783**, 477 (2007).

[20] H. Iida, T. Doi, N. Ishii, H. Suganuma, and K. Tsumura, Prog. Theor. Phys. Suppl. **174**, 238 (2008).

[21] C. J. Morningstar and M. Peardon, Phys. Rev. D **56**, 4043 (1997).

[22] C. J. Morningstar and M. Peardon, Phys. Rev. D **60**, 034509 (1999).

[23] Y. Chen *et al.*, Phys. Rev. D **73**, 014516 (2006).

[24] B. Berg and A. Billoire, Nucl. Phys. **B221**, 109 (1983).

[25] G. Bali *et al.* (UKQCD Collaboration), Phys. Lett. B **309**, 378 (1993).

[26] C. Michael and M. Teper, Nucl. Phys. **B314**, 347 (1989).

[27] J. Sexton, A. Vaccarino, and D. Weingarten, Phys. Rev. Lett. **75**, 4563 (1995).

[28] M. J. Teper, arXiv:hep-th/9812187.

[29] Yu. A. Simonov, Phys. At. Nucl. **58**, 309 (1995); Yad. Fiz. **58N2**, 357 (1995).

[30] N. O. Agasian, D. Ebert, and E.-M. Ilgenfritz, Nucl. Phys. **A637**, 135 (1998); A. Drago, M. Gibilisco, and C. Ratti, Nucl. Phys. **A742**, 165 (2004).

[31] V. Vento, Phys. Rev. D **75**, 055012 (2007).

[32] P. Petreczky, Nucl. Phys. B, Proc. Suppl. **140**, 78 (2005); F. Karsch, Lect. Notes Phys. **583**, 209 (2002); D. E. Miller, Acta Phys. Pol. B **28**, 2937 (1997).

[33] J. Sollfrank and U. Heinz, Z. Phys. C **65**, 111 (1995); A. Drago, M. Gibilisco, and C. Ratti, Nucl. Phys. **A742**, 165 (2004); B. J. Schaefer, O. Bohr, and J. Wambach, Phys. Rev. D **65**, 105008 (2002); A. Di Giacomo, E. Meggiolaro, Yu. A. Simonov, and A. I. Veselov, Phys. At. Nucl. **70**, 908 (2007).

[34] H. Leutwyler, in *Deconfinemente and Chiral Symmetry in QCD 20 Years Later*, edited by P. M. Zerwas and H. A. Castrup (World Scientific, Singapore, 1993).

[35] N. Ishii, H. Suganuma, and H. Matsufuru, Phys. Rev. D **66**, 094506 (2002); **66**, 014507 (2002); Nucl. Phys. B, Proc. Suppl. **129–130**, 581 (2004).

[36] A. M. Ferrenberg and R. H. Swendsen, Phys. Rev. Lett. **61**, 2635 (1988).

[37] S. Huang *et al.*, Nucl. Phys. B, Proc. Suppl. **17**, 281 (1990).

[38] W. Liu *et al.*, Mod. Phys. Lett. A **21**, 2313 (2006).

[39] Y. Liang, K. F. Liu, B. A. Li, S. J. Dong, and K. Ishikawa, Phys. Lett. B **307**, 375 (1993).

[40] Ph. de Forcrand, M. García Pérez, T. Hashimoto, S. Hioki, H. Matsufuru, O. Miyamura, A. Nakamura, I. O. Stamatescu, T. Takaishi, and T. Umeda (QCD-TARO Collaboration), Phys. Rev. D **63**, 054501 (2001).

[41] T. Umeda, R. Katayama, O. Miyamura, and H. Matsufuru, Int. J. Mod. Phys. A **16**, 2215 (2001).

[42] K. H. Ackermann *et al.* (STAR Collaboration), Phys. Rev. Lett. **86**, 402 (2001).

[43] D. Molnár and M. Gyulassy, Nucl. Phys. **A697**, 495 (2002); **A703**, 893 (2002); D. Molnár, Phys. Rev. Lett. **91**, 092301 (2003).